Alexandria Engineering Journal 104 (2024) 115–123

Contents lists available at ScienceDirect

Alexandria Engineering Journal

journal homepage: www.elsevier.com/locate/aej

Original article

Dust acoustic nonlinearity of nonlinear mode in plasma to compute temporal and spatial results

Aziz Khan [a,b], Muhammad Sinan [c], Sumera Bibi [b], Kamal Shah [d,e], Manel Hleili [f], Bahaaeldin Abdalla [d], Thabet Abdeljawad [d,g,h,i,*]

[a] Department of Physics, University of Malakand, Chakdara, Dir(L) 18000, Khyber Pakhtunkhwa, Pakistan
[b] Department of Physics, Govt. Degree College Mingora, Mingora, Swat 18000, Khyber Pakhtunkhwa, Pakistan
[c] School of Mathematical Sciences, University of Electronic Science and Technology of China, Pidu, Chengdu 611731, Sichuan, China
[d] Department of Mathematics and Sciences, Prince Sultan University, P.O. Box 66833, 11586 Riyadh, Saudi Arabia
[e] Department of Computer Science and Mathematics, Lebanese American University, Byblos, Lebanon
[f] Department of Mathematics, Faculty of Science, University of Tabuk, P.O. Box 741, Saudi Arabia
[g] Department of Medical Research, China Medical University, Taichung 40402, Taiwan
[h] Department of Mathematics and Applied Mathematics, School of Science and Technology, Sefako Makgatho Health Sciences University, Ga-Rankuwa, South Africa
[i] Department of Mathematics Kyung Hee University, 26 Kyungheedae-ro, Dongdaemun-qu Seoul, Republic of Korea

ARTICLE INFO

Keywords:
Approximate solution
Caputo derivative
Reductive perturbation
Homotopy perturbation method

ABSTRACT

Our manuscript is related to use Caputo fractional order derivative (CFOD) to investigate results of non-linear mode in plasma. We establish results for both temporal and spatial approximate solution. For the require results, we use reduction perturbation method (RPM) to find the analytical solution of the dust acoustic shock waves. Further, using the same technique we find the solitary wave potential and compared the solutions obtained with another very useful technique known as Homotopy perturbation method (HPM). The comparison of results for both approaches are more precise and agreed with the exact solution of the problem. Finally, we present graphical representation for different fractional order for both temporal and spatial approximate solution.

1. Introduction

Numerous authors have examined the dust acoustic (DA) waves' nonlinearity [1–7]. The inertialess electron and ions in the dust-electron-ion plasma providing restoring force that can propagate DA nonlinear mode while inertia is provided to the mode by heavy dust particle. Therefore, the linear modes of the dust acoustic are small as compare to the electron and ion thermal speeds [8,9]. Both the compressive solitary waves and the rarefactive waves are generated in the nonlinear regime. Theoretically, according to Ergun et al. [10] these kinds of nonlinear structures are important in the electric fields of the auroral downward zone. The Freja satellite and Viking [11] spacecraft data shows that the electrostatics nonlinear modes are present in the ionospheric magnetic field where each solitary wave have different type of velocities depend on the solitary wave amplitude. When a stationary dust component is present, a novel type of wave mode called the dust ion acoustic (DIA) mode [12] is produced. This mode's phase velocity is somewhere between ion and electron thermal velocities. Boltzmann distributed plasma species have been used to examine the linear and nonlinear dynamics of DA waves in general. However, measurements in the space plasma environment revealed the presence of non-thermally equitable electrons and ions. The fact that these energetic particles are significantly non-thermal has been uncovered. Such particles have been found to cause a divergence from the Boltzmann distribution at high altitudes, in the solar wind, and in many space plasmas [13].

Plasma is the combination of different species like electron, ion (+ve or -ve) may be positron, dust (+ve, -ve) etc. When their is some time external forces like electric field, magnetic field, gravitational field etc, that can be transfer some charged particles from one place to another place and creates a difference of temperature, number density and pressure due to which variety of waves are generated in a plasma. So plasma is not linear in nature, the wave generated in plasma is linear or nonlinear. Most researchers interested in the study of non-linear regimes like to study soliton, shock, dipolar, tripolar, quadropolar vertices and chaos, etc [14–18]. Shock is the type of nonlinear structure that produce in the medium when the waves speed is greater than the speed of sound. The shock waves produce in a medium where

* Corresponding author at: Department of Mathematics and Sciences, Prince Sultan University, P.O. Box 66833, 11586 Riyadh, Saudi Arabia.
E-mail addresses: azizkhanphysics@gmail.com (A. Khan), sinan@std.uestc.edu.cn (M. Sinan), sumeraphysics@gmail.com (S. Bibi), kshah@psu.edu.sa (K. Shah), Mhleili@ut.edu.sa (M. Hleili), babdallah@psu.edu.sa (B. Abdalla), tabdeljawad@psu.edu.sa (T. Abdeljawad).

https://doi.org/10.1016/j.aej.2024.06.030
Received 23 March 2024; Received in revised form 13 May 2024; Accepted 13 June 2024
Available online 22 June 2024

dissipation is greater as compare to dispersion [19–22]. A solitary wave is a dip or hump-shaped structure that moves through a medium with a constant shape and speed. This structure has its own type of amplitude or width, amplitude is related to the strength of the wave or energy while its width to the dispersion property of the wave [23–26]. When in a medium dispersion property is larger as compared to dissipation then solitary wave can be generated.

Fractional calculus (FC) is becoming an indispensable tool for modeling various phenomena in Science and Engineering [27]. FDEs are essential for describing processes related to memory effects. This insight is relatively new, and over the last three to four decades, there has been a rise in active activity investigating different facets of FC and FDEs. The FDEs provide a wealth of modeling and simulation possibilities when compared to integer-order differential equations. The Mittag-Leffler kernel is used by the authors [28] as an approximation solution to the fractional advection–dispersion equation, which is characterized by the fractional derivative. They describe the qualitative characteristics, such as the solution's existence and uniqueness, and conduct their research using the double integration approach. Additionally, they examine how the behavior's fractional order affects the diffusion process.

One popular mathematical tool for studying nonlinear wave phenomena is the reductive perturbation method, sometimes called the numerous scales method. Numerous scientific fields, including as fluid dynamics, plasma physics [29–31], and nonlinear optics, have found use for this technique. The study of nonlinear differential equations makes use of the sophisticated analytical tool known as the homotopy perturbation method (HPM). This approach, which combines the ideas of perturbation theory and homotopy, has drawn a lot of interest from scientists and engineers in a variety of scientific and engineering domains because it can solve nonlinear problems effectively and precisely. The revolutionary work of [32] in his article titled 'Homotopy Perturbation Technique" is credited with the development of the HPM". He suggested building a homotopy with an auxiliary parameter that regulates the solution's convergence as a general framework for solving nonlinear differential equations. The solution to the initial problem can be found by iteratively solving the resulting perturbation equation [33, 34].

The reductive perturbation method and HPM are used in this study while these both methods have shown its efficiency in [35–37] based on Caputo fractional order derivative [38].

Definition 1.1 (*[38]*). Caputo fractional order derivative of a function $f \in C[0,\infty)$ for $\alpha \in (0,1]$ is described by

$$ {}^{c}D_{0+}^{\alpha} f(t) = \frac{1}{\Gamma(1-\alpha)} \int_0^t (t-x)^{-\alpha} f^{(1)}(x)dx. \tag{1}$$

In this article we firstly, compare RPM with HPM technique and using CFOD in the HPM solutions and obtained the temporal as well as spatial solution for the dust acoustic non-linear mode. This article is organized in the following sections. In Section 3 we used Homotopy perturbation method with subsections for temporal and spatial solutions. In these sections we also present its graphical analysis, and at the end we discuss its conclusion.

2. Reduction perturbation method

The basic set of magnetohydrodynamics (MHD) equation that can described the fluid with charges species are the continuity equation to gives the time rate of flow for the dynamics species of the plasma. The dynamics specie in our model is dusts while other species like ion and electrons are consider non-Maxwellian (superthermal).

$$\partial_t n_d + \partial_x (n_d u_d) = 0, \tag{2}$$

In Eq. (2), n_d is the dust density and u_d is the dusts drift in the fluid. Momentum equation in the MHD equation described the dynamics of the dusts, is given by,

$$\partial_t u_d + u_d \partial_x u_d + e\partial_x \phi = 0, \tag{3}$$

Eq. (3) ϕ is the perturbed potential and moment of the dust is taken in one dimension that is x-axis. Due to the charge in equation how much potential is created in the plasma is described by the Poisson's equation

$$\partial_x^2 \phi = (\mu n_e - Z_d n_d - \delta n_i). \tag{4}$$

Eq. (4) has some parameter like n_e electron density, Z_d dust charge number, $\mu = n_{i0}/Z_{d0}n_{d0}$, and $\delta = n_{e0}/Z_{d0}n_{d0}$. According to Kappa distribution the number density of electron and ion in the plasma can be written as

$$\begin{aligned} n_e &= \left[1 - \frac{\Phi}{(\kappa_e - 3/2)}\right]^{1/2-\kappa_e} \\ n_i &= \left[1 - \frac{\tau_1 \Phi}{(\kappa_i - 3/2)}\right]^{1/2-\kappa_i}. \end{aligned} \tag{5}$$

In the given set of equations, e, Φ, T_e, T_i, κ_e, and κ_i are the electron/ion charge, perturbed potential, electron, ion temperature and special index for the electron and ion kappa distribution, in that order. Moreover n_{e0}, n_{i0}, n_{d0}, and Z_{e0} are the unperturbed number densities of electron, ion, dust and unperturbed charge of the dust particle. Using the stretching coordinates as follow by Taniuti and Washimi [26], $\xi = \epsilon^{\frac{1}{2}}\left(\frac{x}{\lambda_0} - t\right)$, $\tau = \epsilon^{\frac{3x}{2}}$. Also $\epsilon > 0$ is a small parameter in the stretching coordinates which shows the delicacy of amplitude and λ_0 is the phase velocity of the wave. The different parameters of plasma can be written in the power series of infinitesimal parameter ϵ as;

$$X = \sum_{n=0}^{\infty} \epsilon^n X^{(n)} \tag{6}$$

Where, X may be n_d, u_d, ϕ, and Z_d while, in the given series u_d^0, and ϕ^0 are zeros in value and n_d and Z_d are non-zero. Using (2)–(6) by comparing $\epsilon^{(1)}$ both sides of the equations, we can write continuity equation as

$$-\partial_\xi n_d + \frac{1}{\lambda_0}\partial_\xi (n_d u_d) + \epsilon \partial_\tau n_d u_d = 0, \tag{7}$$

the momentum equation

$$-\partial_\xi u_d + \frac{u_d}{\lambda_0}\partial_\xi u_d + \epsilon u_d \partial_\tau u_d + \frac{Z_d}{\lambda_0}\partial_\xi \Phi + \epsilon Z_d \partial_\tau \Phi = 0, \tag{8}$$

and Poisson's equation

$$\frac{\epsilon}{\lambda_0^2}\partial_\xi^2 \Phi + \frac{2\epsilon^2}{\lambda_0}\partial_{\xi\tau}^2 \Phi + \epsilon^3 \partial_\tau^2 \Phi = \mu a_e^\kappa e^{\Phi} - Z_d n_d - \delta a_i^\kappa e^{-\Phi}. \tag{9}$$

Where, $a_e^\kappa = (\kappa - 1)/(k - 3/2)$ $a_i^\kappa = \tau a_e^\kappa$, and $\tau_1 = T_e/T_i$. The next higher order with respect to ϵ in our reductive perturbation method, we can write equation of continuity as

$$-\partial_\xi u_d^{(2)} + \frac{n_d^{(0)}}{\lambda_0}\partial_\xi n_d^{(2)} + \frac{1}{\lambda_0}\partial_\xi (n_d^{(1)} u_d^{(1)}) + \partial_\tau (n_d^{(1)} u_d^{(1)}) = 0, \tag{10}$$

the dust momentum equation

$$-\partial_\tau u_d^{(2)} + \frac{Z_d^{(0)}}{\lambda_0}\partial_\xi \Phi^{(2)} + \frac{u_d^{(1)}}{\lambda_0}\partial_\xi u_d^{(1)} + Z_d^{(0)}\partial_\tau \Phi + \eta_v \partial_\xi^2 \Phi = 0, \tag{11}$$

here η_v is the coefficient of dissipative effect in plasma.

$$\frac{1}{\lambda_0^2}\partial_\xi^2 \Phi - a_e^\kappa(\sigma_i + 1)\Phi^{(2)} + Z_d^{(0)} n_d^{(2)} = 0. \tag{12}$$

By coupling (8)–(12), we can get the generalized non-linear partial differential in the form of

$$\partial_\tau \Phi + A\Phi\partial_\xi \Phi + B\partial_\xi^3 \Phi + C\partial_\xi^2 \Phi = 0. \tag{13}$$

We have neglected the second order perturbed potential in our calculation.

2.1. Shock by reduction perturbation method

The non-linear structure just like a shock can be obtained in a medium by neglecting dispersive effect as compared to dissipation. From (13), when we neglect B coefficient term then we can get non-linear partial differential equation (PDE) in the form of

$$\partial_\tau \Phi + A\Phi\partial_\xi \Phi + C\partial_\xi^2 \Phi = 0. \tag{14}$$

The exact solution of non-linear PDE Eq. (14) is given as

$$\Phi = \Phi_m \left(1 - \tanh\left(\frac{\xi}{\triangle}\right)\right), \tag{15}$$

where $\triangle = 2C/u_0$ is the width and $\Phi_m = u_0/A$ is the shock wave amplitude.

2.2. Soliton by reduction perturbation method

When we neglected the dispersion greater as compared to dissipative effect in the fluid then Eq. (13) can be written as,

$$\partial_\tau \Psi + A\Psi\partial_\xi \Psi + B\partial_\xi^3 \Psi = 0. \tag{16}$$

The exact solution of the corresponding Eq. (16) is given as

$$\Psi = \Psi_0 Sech^2\left(\frac{\xi}{\triangle^1}\right), \tag{17}$$

where, $\Psi_0 = u_0/A$, and $\triangle^1 = \sqrt{4B/u_0}$ are the amplitude and width of the corresponding non-linear structure (soliton).

3. Solution by homotopy perturbative method

Korteweg–de-Vries (KdV) burger type of equation is given as

$$\frac{\partial \Phi}{\partial t} + A\Phi\frac{\partial \Phi}{\partial \xi} - C\frac{\partial^2 \Phi}{\partial \xi^2} = 0, \tag{18}$$

to solve (18) by Homotopy Perturbative Method (HPM) method we will follow the following method. Generally homotopy for a given nonlinear differential equation can be written with fractional derivative as

$$H(\Phi, t) = \frac{\partial^\alpha}{\partial t^\alpha}\Phi - \frac{\partial^\alpha}{\partial t^\alpha}\Phi_0 + p\frac{\partial^\alpha}{\partial t^\alpha}\Phi_0 + p\left(A\Phi\frac{\partial^\beta}{\partial \xi^\beta}\Phi - C\frac{\partial^{2\beta}}{\partial \xi^{2\beta}}\Phi\right) = 0, \tag{19}$$

taking solution of the Eq. (18) in the form of a power series as,

$$\Phi(\xi, t) = \sum_{n=0}^{\infty} p^n \Phi^{(n)}, \tag{20}$$

where p is the small perturbation parameter, Φ^n is the corresponding potential associated due to the different perturbation and n has an integer having values of $\{0, 1, 2, 3, \dots\}$. When put equation Eq. (20) in (19) and compare different power of p to both hand sides of Eq. (19) we can get as

$$\left.\begin{aligned}
p^0 &:= \frac{\partial^\alpha}{\partial t^\alpha}\Phi^{(0)} = \frac{\partial^\alpha}{\partial t^\alpha}\Phi^{(0)},\\
p^1 &:= \frac{\partial^\alpha}{\partial t^\alpha}\Phi^{(1)} + A\Phi^{(0)}\frac{\partial^\beta}{\partial \xi^\beta}\Phi^{(0)} - C\frac{\partial^{2\beta}}{\partial \xi^{2\beta}}\Phi^{(0)} = 0,\\
p^2 &:= \frac{\partial^\alpha}{\partial t^\alpha}\Phi^{(2)} + A\Phi^{(1)}\frac{\partial^\beta}{\partial \xi^\beta}\Phi^{(1)} - C\frac{\partial^{2\beta}}{\partial \xi^{2\beta}}\Phi^{(1)} = 0,\\
p^3 &:= \frac{\partial^\alpha}{\partial t^\alpha}\Phi^{(3)} + A\Phi^{(2)}\frac{\partial^\beta}{\partial \xi^\beta}\Phi^{(2)} - C\frac{\partial^{2\beta}}{\partial \xi^{2\beta}}\Phi^{(2)} = 0,\\
p^4 &:= \frac{\partial^\alpha}{\partial t^\alpha}\Phi^{(4)} + A\Phi^{(3)}\frac{\partial^\beta}{\partial \xi^\beta}\Phi^{(3)} - C\frac{\partial^{2\beta}}{\partial \xi^{2\beta}}\Phi^{(3)} = 0,\\
&\vdots
\end{aligned}\right\} \tag{21}$$

For complete solution of KDV burger equation (18), we obtain various order of potential, then using Eq. (20) to get the desired result.

3.1. Temporal solution of the KdV-Burger equation

Take the initial condition for the temporal solution as,

$$\Phi^{(0)} = \Phi^{(0)}. \tag{22}$$

For the HPM method we have required some initial condition to get the approximate solution of the given nonlinear PDE, so we assume our initial condition of the form as

$$\Phi^{(0)} = \Phi_m \left[1 - \tanh\left(\frac{\xi}{\triangle}\right)\right], \tag{23}$$

Where $\triangle = \frac{2c}{U_0}$ so unperturbed and the next (first, second and ... so on) order perturbed potential for the shock wave will be obtained as

$$\left.\begin{aligned}
\Phi^0 &= \Phi^{(0)},\\
\Phi^1 &= -\left(A\Phi^{(0)}\frac{\partial^\beta}{\partial \xi^\beta}\Phi^{(0)} - C\frac{\partial^{2\beta}}{\partial \xi^{2\beta}}\Phi^{(0)}\right)\frac{t^\alpha}{\Gamma(\alpha+1)},\\
\Phi^2 &= -\left(A\Phi^{(1)}\frac{\partial^\beta}{\partial \xi^\beta}\Phi^{(1)} - C\frac{\partial^{2\beta}}{\partial \xi^{2\beta}}\Phi^{(1)}\right)\frac{t^\alpha}{\Gamma(\alpha+1)},\\
\Phi^3 &= -\left(A\Phi^{(2)}\frac{\partial^\beta}{\partial \xi^\beta}\Phi^{(2)} - C\frac{\partial^{2\beta}}{\partial \xi^{2\beta}}\Phi^{(2)}\right)\frac{t^\alpha}{\Gamma(\alpha+1)},\\
\Phi^4 &= -\left(A\Phi^{(3)}\frac{\partial^\beta}{\partial \xi^\beta}\Phi^{(3)} - C\frac{\partial^{2\beta}}{\partial \xi^{2\beta}}\Phi^{(3)}\right)\frac{t^\alpha}{\Gamma(\alpha+1)},\\
&\vdots
\end{aligned}\right\} \tag{24}$$

First order problem

By comparing the first order perturbed potential we have as,

$$\Phi^1 = -\left(A\Phi^{(0)}\frac{d}{d\xi}\Phi^{(0)} - C\frac{d^2}{d\xi^2}\Phi^{(0)}\right)\frac{t^\alpha}{\Gamma(\alpha+1)}. \tag{25}$$

implies that

$$\begin{aligned}
\Phi^1 = {} & \frac{t^\alpha \Phi_m^2}{\triangle\,\Gamma(\alpha+1)}\left(1 - \tanh\left(\frac{\xi}{\triangle}\right)^2\right)\\
& \times \left\{A\left(1 - \tanh\left(\frac{\xi}{\triangle}\right)\right) + \frac{2C}{\triangle^2}\left(1 - 3\tanh\left(\frac{\xi}{\triangle}\right)^2\right)\right\},
\end{aligned} \tag{26}$$

the complete temporal solution for KdV-burger equation is,

$$\Phi = \Phi^0 + \Phi^1 + \cdots$$

$$\begin{aligned}
\Phi = {} & \Phi_m\left[1 - tanh\left(\frac{\xi}{\triangle}\right)\right] + \frac{t^\alpha \Phi_m^2}{\triangle\,\Gamma(\alpha+1)}\left(1 - \tanh\left(\frac{\xi}{\triangle}\right)^2\right)\\
& \times \left\{A\left(1 - \tanh\left(\frac{\xi}{\triangle}\right)\right) + \frac{2C}{\triangle^2}\left(1 - 3\tanh\left(\frac{\xi}{\triangle}\right)^2\right)\right\} + \cdots
\end{aligned} \tag{27}$$

3.2. Spatial solution of the KdV-Burger equation

By comparing the first order perturbed potential we have as,

$$\Phi^1 = -\left(A\Phi^{(0)}\frac{\partial^\beta}{\partial \xi^\beta}\Phi^{(0)} - C\frac{d^3}{d\xi^3}\Phi^{(0)}\right)\frac{t^\alpha}{\Gamma(\alpha+1)}. \tag{28}$$

The complete spatial solution for the shock wave is,

$$\begin{aligned}
\Phi = {} & \Phi_m\left[1 - tanh\left(\frac{\xi}{\triangle}\right)\right] - \frac{A\Phi_m^2 t^\alpha}{\xi^\beta\,\Gamma(\alpha+1)}\left(1 - \tanh\left(\frac{\xi}{\triangle}\right)\right)\\
& \times \left\{\frac{1}{\Gamma(1-\beta)} - \frac{\xi}{\triangle\,\Gamma(2-\beta)} + \frac{2\xi^3}{\triangle^3\,\Gamma(4-\beta)}\right\}\\
& + \frac{2Ct^\alpha \Phi_m}{\triangle^3\cosh\left(\frac{\xi}{\triangle}\right)^4\Gamma(\alpha+1)}\left\{3 - 2\cosh\left(\frac{\xi}{\triangle}\right)^2\right\}.
\end{aligned} \tag{29}$$

The Eq. (29), is plotted in the next plots, that are given below.

3.3. Electric field

By using $E=-\nabla\Psi$, we can fine the electric field corresponding to each solution obtained for the shock as well as solitary waves. Electric field for the solitary wave is,

$$E=\frac{A\Phi_m^2 t^\alpha}{\triangle^2\,\Gamma(\alpha+1)}\left(1-\tanh\left(\frac{\xi}{\triangle}\right)^2\right)\left\{1+2\tanh\left(\frac{\xi}{\triangle}\right)-3\tanh\left(\frac{\xi}{\triangle}\right)^2\right\}+\frac{8B\Phi_m}{\triangle^4}\tanh\left(\frac{\xi}{\triangle}\right)\left(1-\tanh\left(\frac{\xi}{\triangle}\right)^2\right)\times\left\{\tanh\left(\frac{\xi}{\triangle}\right)^2-2\left(1-\tanh\left(\frac{\xi}{\triangle}\right)\right)\right\}-\frac{\Phi_m}{\triangle}\left(1-\tanh\left(\frac{\xi}{\triangle}\right)^2\right). \tag{30}$$

The plot for Eq. (30) is given here as,

3.4. Solitary wave potential

This part is divided in to some sub portions.

3.4.1. Temporal soliton

Initial condition for the temporal solution is,

$$\Psi^{(0)}=\Psi^{(0)}. \tag{31}$$

For the HPM method we have required some initial condition to get the approximate solution of the given nonlinear PDE, so we assume our initial condition of the form as

$$\Psi^{(0)}=\Psi_m sech\left(\frac{\xi}{W}\right)^2, \tag{32}$$

where $W=\sqrt{4B/U}$ so unperturbed and the next (first, second and ... so on) order perturbed potential for the shock wave will be obtained as

$$\left.\begin{aligned}
\Psi^0 &= \Psi^{(0)},\\
\Psi^1 &= -\left(A\Psi^{(0)}\frac{\partial^\beta}{\partial\xi^\beta}\Psi^{(0)}+B\frac{\partial^{3\beta}}{\partial\xi^{3\beta}}\Psi^{(0)}\right)\frac{t^\alpha}{\Gamma(\alpha+1)},\\
\Psi^2 &= -\left(A\Psi^{(1)}\frac{\partial^\beta}{\partial\xi^\beta}\Psi^{(1)}+B\frac{\partial^{3\beta}}{\partial\xi^{3\beta}}\Psi^{(1)}\right)\frac{t^\alpha}{\Gamma(\alpha+1)},\\
\Psi^3 &= -\left(A\Psi^{(2)}\frac{\partial^\beta}{\partial\xi^\beta}\Psi^{(2)}+B\frac{\partial^{3\beta}}{\partial\xi^{3\beta}}\Psi^{(2)}\right)\frac{t^\alpha}{\Gamma(\alpha+1)},\\
\Psi^4 &= -\left(A\Psi^{(3)}\frac{\partial^\beta}{\partial\xi^\beta}\Psi^{(3)}+B\frac{\partial^{3\beta}}{\partial\xi^{3\beta}}\Psi^{(3)}\right)\frac{t^\alpha}{\Gamma(\alpha+1)},\\
&\vdots
\end{aligned}\right\} \tag{33}$$

First order problem

$$\Psi^1=-\left(A\Psi^{(0)}\frac{d}{d\xi}\Psi^{(0)}+B\frac{d^3}{d\xi^3}\Psi^{(0)}\right)\frac{t^\alpha}{\Gamma(\alpha+1)}, \tag{34}$$

implies that

$$\Psi^1=\frac{2\Psi_m t^\alpha}{W\Gamma(\alpha+1)}sech\left(\frac{\xi}{W}\right)^2\tanh\left(\frac{\xi}{W}\right)\times\left[A\Psi_m sech\left(\frac{\xi}{W}\right)^2-\frac{4B}{W^2}\left\{2-3\tanh\left(\frac{\xi}{W}\right)^2\right\}\right], \tag{35}$$

which further gives the complete temporal solution for the solitary wave is,

$$\Psi=\Psi^0+\Psi^1+\cdots$$

$$\Psi=\Psi_m sech\left(\frac{\xi}{W}\right)^2+\frac{2\Psi_m t^\alpha}{W\Gamma(\alpha+1)}sech\left(\frac{\xi}{W}\right)^2\tanh\left(\frac{\xi}{W}\right)\times\left[A\Psi_m sech\left(\frac{\xi}{W}\right)^2-\frac{4B}{W^2}\left\{2-3\tanh\left(\frac{\xi}{W}\right)^2\right\}\right]+\cdots \tag{36}$$

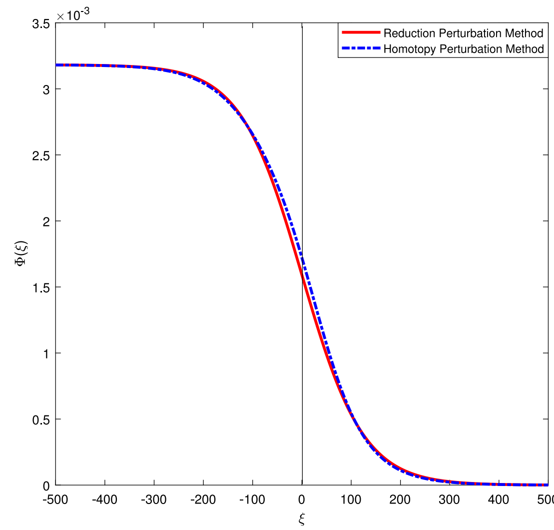

Fig. 1. Comparison of 2D fractional temporal numerical solution $\Phi(\xi)$ by HPM with RPM exact solution for order $\alpha=1.0$ and $t=40$ s based on Eqs. (15) and (27).

This equation shows the solitary wave potential with some extra terms, the superpose terms indicates the time factor with fractional order. Here we can say that when we take the time limit larger the superpose terms will produce dominant effect but for smaller time limit the shape of the solitary waves is resemble to the analytical solution. The solution for Eq. (36) is plotted from which we can get important compression and fractional solution for the same structure.

3.4.2. Spatial solution of the KdV equation

Comparing the first order of the potential through spatial calculation, we have,

$$\Psi^1=-\left(A\Psi^{(0)}\frac{d^\beta}{d\xi^\beta}\Psi^{(0)}+B\frac{d^3}{d\xi^3}\Psi^{(0)}\right)\frac{t^\alpha}{\Gamma(\alpha+1)}, \tag{37}$$

$$\Psi^1=\frac{8B\Psi_m}{W^3}sech\left(\frac{\xi}{W}\right)^2\tanh\left(\frac{\xi}{W}\right)\left\{2\tanh\left(\frac{\xi}{W}\right)^2-2\right\}-\frac{2A\Psi_m^2}{\xi^\beta}sech\left(\frac{\xi}{W}\right)^2\left\{\frac{1}{\Gamma(1-\beta)}-\frac{2\xi^2}{W^2\Gamma(3-\beta)}+\frac{16\xi^4}{W^4\Gamma(5-\beta)}\right\}. \tag{38}$$

In Eq. (38) beta is the spatial fractional factor by varying this factor we can change the dynamics of the solitary wave. These variation are given here,

3.4.3. Electric field

By using $E=-\nabla\Psi$, we can fine the electric field of the solitary wave as,

$$E=-\frac{2\Psi_m \mathrm{sech}(\frac{x}{W})^2\tanh(\frac{x}{W})}{W}+\frac{8A\Psi_m^2}{W^2}sech\left(\frac{\xi}{W}\right)^4\times\left\{5\tanh\left(\frac{\xi}{W}\right)^2-1\right\}+\frac{8B\Psi_m}{W^4}sech\left(\frac{\xi}{w}\right)^2\left\{2-15\tanh\left(\frac{\xi}{W}\right)^2+15\tanh\left(\frac{\xi}{W}\right)^4\right\}. \tag{39}$$

Different plots for the solitary wave electric field are shown graphically, its discussion is given in the result and discussion section.

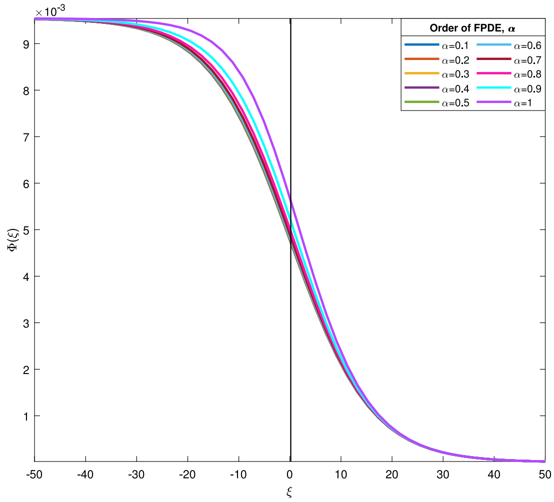

Fig. 2. 2D fractional temporal numerical solution $\Phi(\xi)$ for $t = 40$ s.

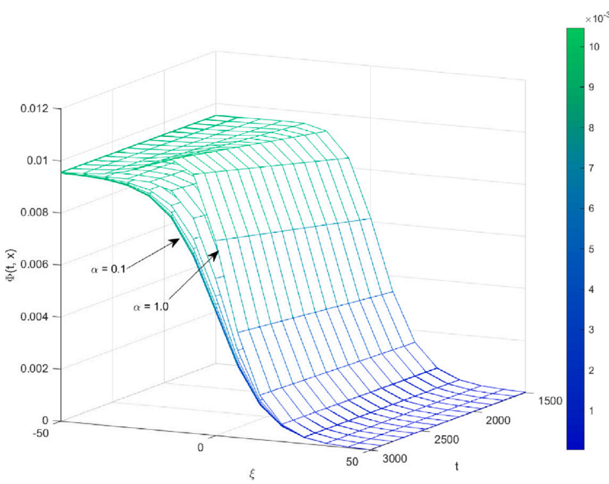

Fig. 3. 3D fractional temporal numerical solution $\Phi(t, \xi)$ for order $\alpha \in (0, 1]$.

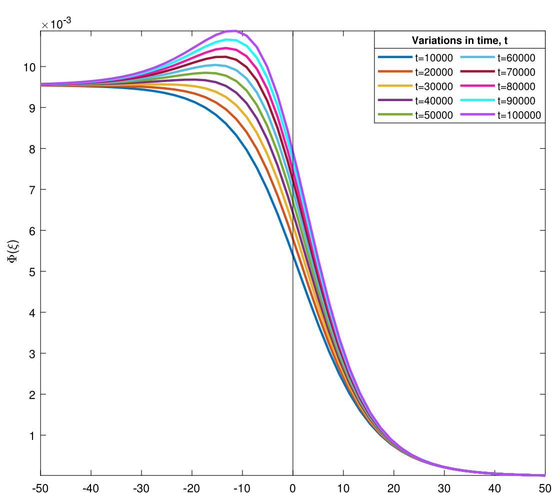

Fig. 4. 2D fractional temporal numerical solution $\Phi(\xi)$ for order $\alpha = 0.7$.

4. Results and discussion

Fig. 1 red solid plot shows the solution of dust acoustic wave by reductive pertebative method while the blue dot dashed plot is the solution of shock by homotopy perturbation method in the time limit of $t = 40$ s. When we increase the time limit the deviation b/w the reductive pertebative method and homotopy perturbation method is increases, reductive pertebative method gives its calculation simple and closer to the exact value. Fig. 2 we have discuss the 2D shock wave potential against ξ for different value of α (where α is the order of Caputo fractional order derivative (CFOD), the spectra different $\Phi(\xi)$ with respect to α gives us that we can take any value of α within the range of $(0, 1]$ for our solution. While our simulation goes to exact solution when we take $\alpha = 1$. Fig. 3 shows us the simulation of shock wave potential against ξ and time t. Where we have plot all the solution for $\alpha = (0, 1]$ range and the time variation in the simulation shows that the small value of time gives us the exact solution by homotopy perturbation method while the solution is deviated when we goes to higher value of time. Fig. 4 shows the 2D simulation for different value of time that gives the same behavior which is discussed in the previous Fig. 3. Fig. 5 is the contour plot of shock waves potential against time t and ξ.

In Fig. 6 the red solid plot shows the shock wave potential by reductive pertebative method, where the blue dot dashed plot shows the shock wave potential spatial solution using homotopy perturbation method for order $\alpha = 1$, $\beta = 1$ and $t = 0.1$ s. This comparison concludes that within very small time limit the solution by homotopy perturbation method converges to reductive pertebative method.

In Fig. 7 we have drawn the spatial potential of shock wave vs. ξ and time t, for $\alpha = 0.7$ and β (spatial fractional order) in range $[0.1, 0.4]$ based on Eq. (29). Simulation shows that the shock potential amplitude enhances with the value of β. While in Fig. 8 the plot is electric field vs. ξ for time $t = 0.01$ shows variations with order α. In Fig. 9 is the comparison of temporal solution of solitary wave potential, the red solid plot is by reductive pertebative method and the blue dot dashed plot is by homotopy perturbation method, for $\alpha = 1$ and time $t = 1 \times 10^3$ while keeping all the parameter constant. These two approaches are very close to each other as shown in the corresponding simulation. In Fig. 10 is 2D plot among solitary wave potential vs. ξ for time $t = 1 \times 10^2$. Observations show that within $\alpha \in (0.1, 1]$ the solution of solitary wave potential are valid, the solution gives its exact simulation when we take $\alpha = 1$. While Fig. 11 is the 3D plot of solitary temporal solution vs. time t and ξ and Fig. 12 is the soliton contour plot against time t and ξ. Fig. 13 is the solitary wave potential (spatial), here the solid red plot is for reductive pertebative method and blue dot dashed plot is for HPM, for $\alpha = 1$, $\beta = 1$ and time $t = 1 \times 10^3$ while keeping all the other parameters constant. The two different approaches are closed to one another when time is taken small. But we have also observed that for time greater than 1×10^3 both approaches mismatched to one another. Fig. 14 is the 2D plot of spatial solitary wave potential against ξ for order $\alpha = 1$ and $\beta \in [0.2, 1]$. Observation shows that for $\beta = 1$ the plot gives the exact shape of solitary wave potential but for value less than 1 the plot shape distort at the peak value of the solitary wave potential while its width remains unchanged. It means that the variation with β changes the amplitude of the soliton wave potential but its disruption property is not affected.

In Fig. 15 is the 3D simulation of spatial solitary wave potential against time t and ξ for $\alpha = 1$. The variation which we have mentioned for figure Fig. 14 is clear from that plot. While Fig. 16 is the contour plot of soliton potential against time t and ξ. We have used the following parameters which are mentioned in the previous literature [15,21,22] such that $n_e = 1$, $\sigma_i = 0.1$, $n_i = 0.1$, $u = 0.001$, $Z_d = 0.8$, $n_d = 0.01$, $\sigma_d = 0.001$, $r_d = 1.2$, $p_d = 1$, and $k \in [1, 5]$.

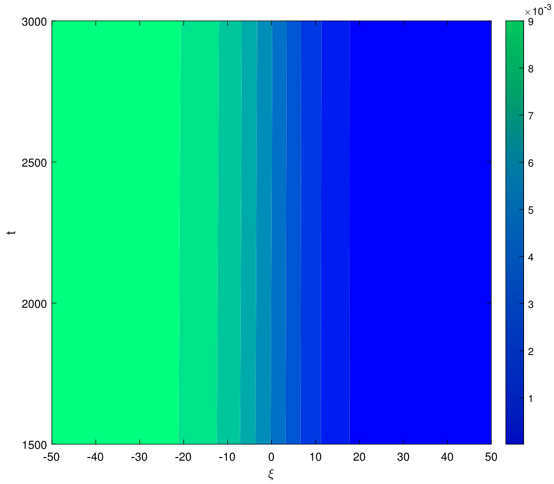

Fig. 5. Contour plot of $\Phi(\xi, t)$ vs t and ξ.

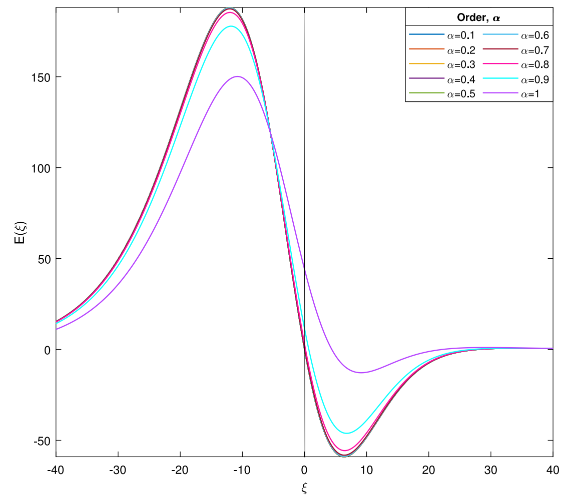

Fig. 8. 2D fractional temporal numerical solution $E(x, t)$ for order $t = 0.01$.

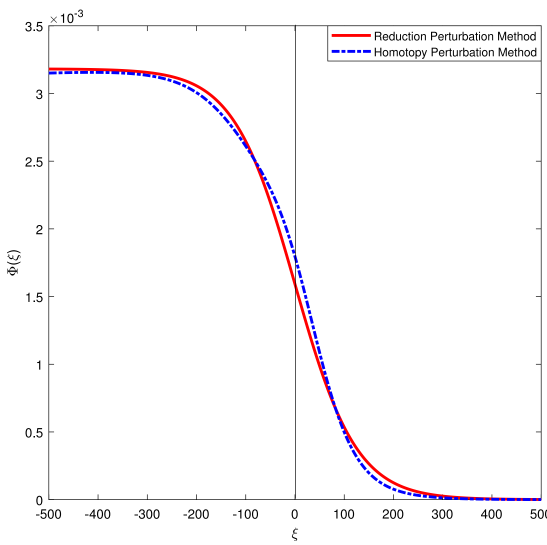

Fig. 6. Comparison of 2D fractional spatial numerical solution $\Phi(\xi)$ by HPM with RPM exact solution for order $\alpha = 1.0$, $\beta = 1$, and $t = 0.1$ s based on Eqs.(15) and (29).

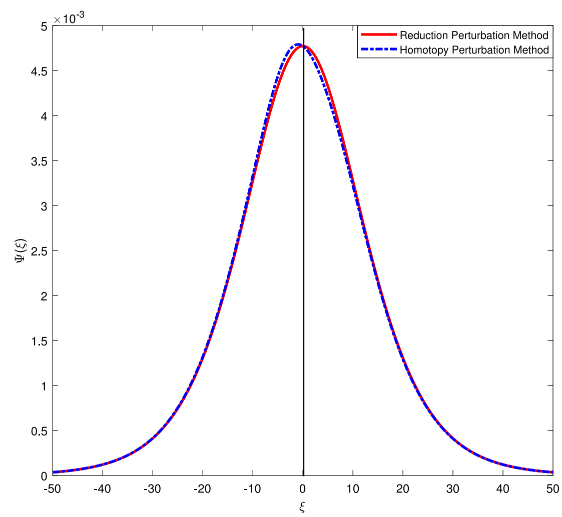

Fig. 9. Comparison between RPM and HPM of temporal Solution for order $\alpha = 1.0$ and $t = 1 \times 10^3$, based on Eqs. (17) and (36).

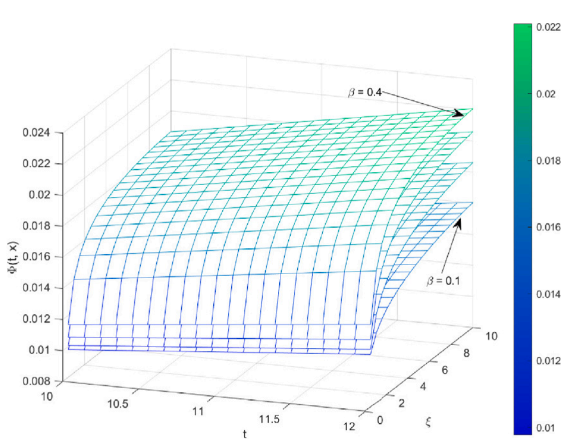

Fig. 7. 3D fractional spatial numerical solution $\Phi(t, \xi)$ for order $\alpha = 0.7$.

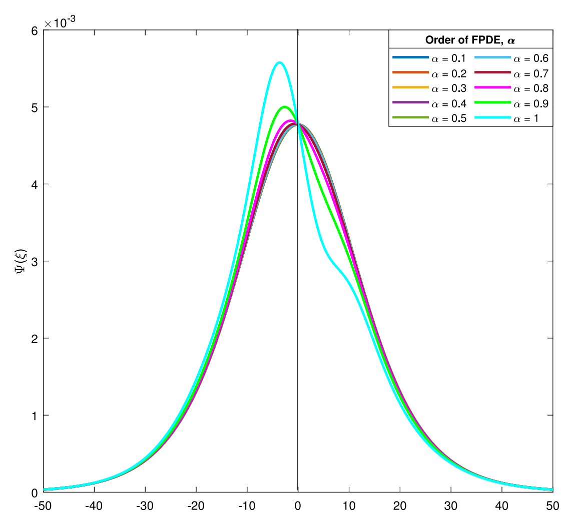

Fig. 10. 2D fractional temporal numerical solution $\Psi(\xi)$ for time $t = 1 \times 10^2$.

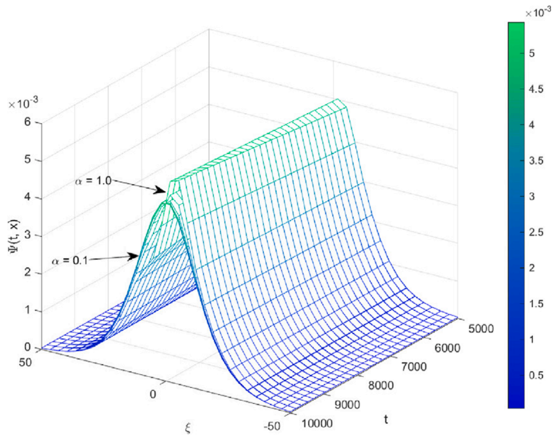

Fig. 11. 3D plot of fractional temporal numerical solution $\Psi(\xi, t)$ vs t and ξ, based on Eq. (36).

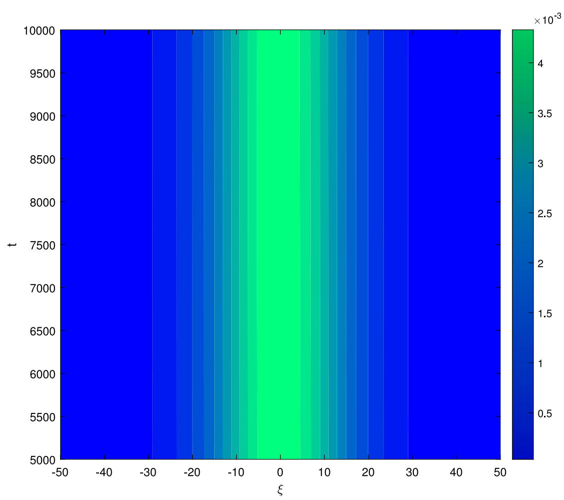

Fig. 12. Contour plot of fractional temporal numerical solution $\Psi(\xi, t)$ vs time t and ξ, based on Eq. (36).

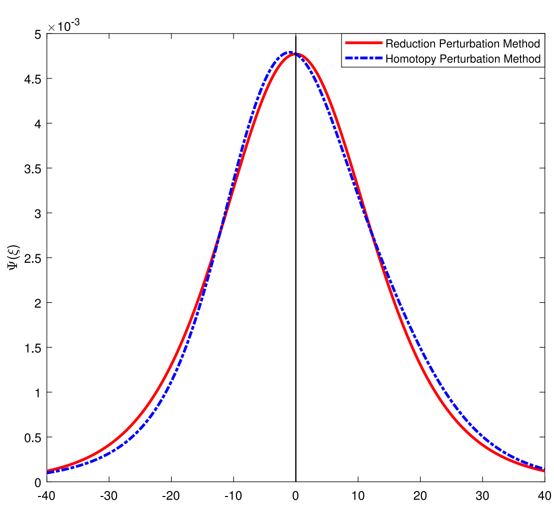

Fig. 13. Comparison between RPM and HPM of spatial Solution for order $\alpha = 1.0$, $\beta = 1.0$ and $t = 1 \times 10^3$, based on Eqs. (17) and (38).

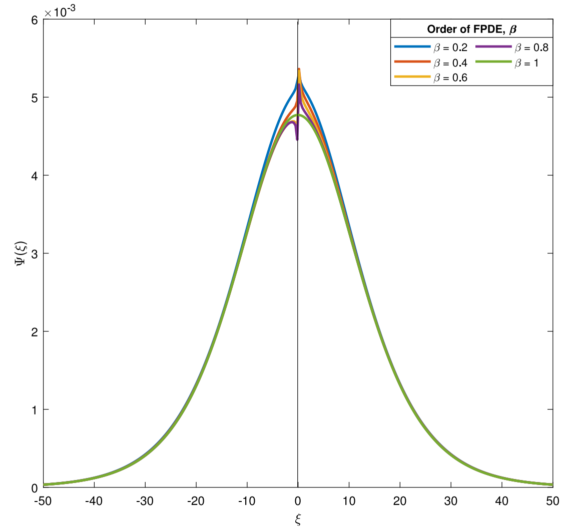

Fig. 14. 2D fractional spatial numerical solution $\Psi(\xi)$ vs ξ for order $\alpha = 1.0$.

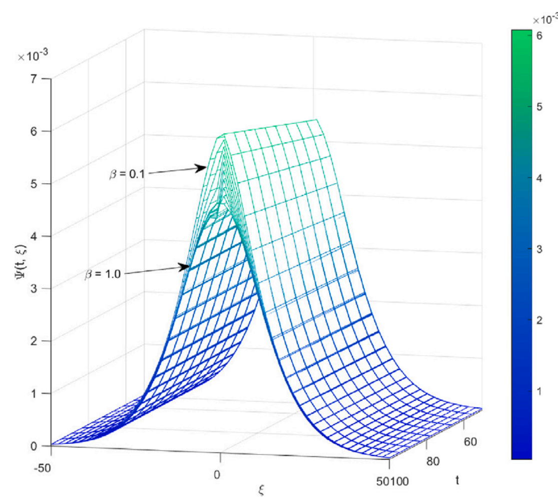

Fig. 15. 3D fractional spatial numerical solution $\Psi(\xi, t)$ plot vs time t and ξ for $\alpha = 1.0$, based on Eq. (38).

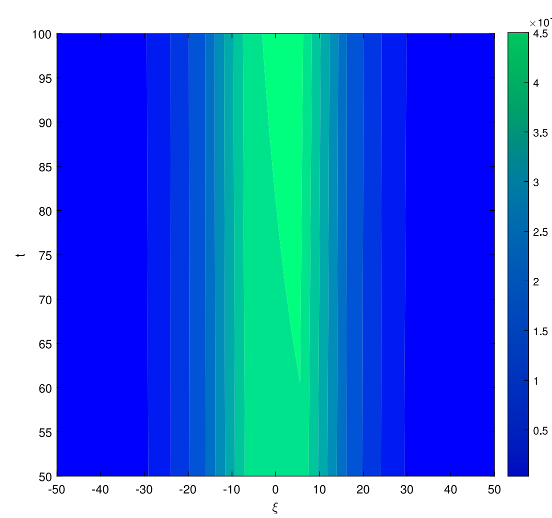

Fig. 16. Contour plot of fractional spatial numerical solution $\Psi(\xi, t)$ vs time t and ξ for $\alpha = 1.0$, based on Eq. (38).

5. Conclusions

Our work concentrated on applying the reductive perturbation method and the homotopy perturbation method, two analytical techniques, to the study of electron-ion and dust plasma dynamics. In addition to treating ions and electrons as dynamic species, we also treated dust as one. A series of continuity, momentum, and Poisson equations for the dust species in the plasma were among the magnetohydrodynamic equations to which the reductive perturbation method was applied. KdV Burger and KdV equations were the two kind of solutions that were computed as a result. Furthermore, we used the Caputo fractional order derivatives in the homotopy perturbation approach to get two distinct solutions for the KdV Burger equation and the KdV equation. For the solitary wave potential, we were able to get both temporal and spatial solutions. Reduction and homotopy perturbation techniques, in particular, coincided within a shorter time limit, and the temporal fractional order (α) and spatial fractional order (β) had an impact on the solutions. We noticed that the solutions got closer to classical order solutions as the value of α grew toward 1. In a similar vein, the solutions approximated classical order solutions when the spatial fractional order (β) approached 1. Moreover, we observed that the amplitude of the structures did not change, but the width was influenced by the temporal fractional order. Conversely, the forms' amplitude was impacted by the spatial fractional order, but the width remained constant. Our results showed that the homotopy perturbation approach and the reductive perturbation method are useful tools for studying dust and electron-ion plasma dynamics. The solutions were shaped by the fractional orders (α and β), which had an impact on the amplitude and width of the structures. These findings shed light on the behavior of the system under study and advance our knowledge of plasma dynamics.

CRediT authorship contribution statement

Aziz Khan: Formal analysis, Data curation. **Muhammad Sinan:** Software, Methodology. **Sumera Bibi:** Methodology, Investigation, Formal analysis. **Kamal Shah:** Conceptualization. **Manel Hleili:** Conceptualization, Formal analysis. **Bahaaeldin Abdalla:** Supervision, Visualization. **Thabet Abdeljawad:** Validation, Supervision.

Declaration of competing interest

The authors declare that they have no known competing financial interests or personal relationships that could have appeared to influence the work reported in this paper.

Data availability statement

The data used has included within the paper.

Acknowledgment

The authors would like to thank Prince Sultan University for APC and support through the TAS research lab.

References

[1] R.L. Merlino, A. Barkan, C. Thompson, N. D'angelo, Laboratory studies of waves and instabilities in dusty plasmas, Phys. Plasmas 5 (5) (1998) 1607–1614.
[2] P. Shukla, A survey of dusty plasma physics, Phys. Plasmas 8 (5) (2001) 1791–1803.
[3] P.K. Shukla, B. Eliasson, Colloquium: Fundamentals of dust-plasma interactions, Rev. Modern Phys. 81 (1) (2009) 25.
[4] S.Z. Li, W.T. Huang, J. Zhang, D. Wang, Discharge characteristics of an atmospheric-pressure argon plasma column generated with a single-electrode configuration, Phys. Plasmas 16 (7) (2009) 073503.
[5] A. Misra, N. Adhikary, Electrostatic solitary waves in dusty pair-ion plasmas, Phys. Plasmas 20 (10) (2013) 102309.
[6] A. Saha, P. Chatterjee, N. Pal, Nonlinear dust acoustic travelling waves in dusty plasmas due to dust charge fluctuations, J. Plasma Phys. 81 (5) (2015) 905810509.
[7] N. Rao, P. Shukla, M.Y. Yu, Dust-acoustic waves in dusty plasmas, Planet. Space Sci. 38 (4) (1990) 543–546.
[8] M. Emamuddin, S. Yasmin, A. Mamun, Higher order nonlinear equations for the dust-acoustic waves in a dusty plasma with two temperature-ions and nonextensive electrons, Phys. Plasmas 20 (4) (2013) 043705.
[9] M. Emamuddin, M. Masud, A. Mamun, Dust-acoustic solitary waves in a magnetized dusty plasmas with nonthermal ions and two-temperature nonextensive electrons, Astrophys. Space Sci. 349 (2014) 821–828.
[10] R. Ergun, C. Carlson, L. Muschietti, I. Roth, J. McFadden, Properties of fast solitary structures, Nonlinear Process. Geophys. 6 (3/4) (1999) 187–194.
[11] A. Mamun, B. Eliasson, P. Shukla, Three-dimensional electroacoustic solitary waves induced by ion holes in magnetized plasmas, Phys. Plasmas 11 (9) (2004) 4535–4538.
[12] P. Shukla, V. Silin, Dust ion-acoustic wave, Phys. Scr. 45 (5) (1992) 508.
[13] M.D. Montgomery, S. Bame, A. Hundhausen, Solar wind electrons: Vela 4 measurements, J. Geophys. Res. 73 (15) (1968) 4999–5003.
[14] H.U. Rehman, I. Iqbal, S. Subhi Aiadi, N. Mlaiki, M.S. Saleem, Soliton solutions of Klein–Fock–Gordon equation using Sardar subequation method, Mathematics 10 (18) (2022) 3377.
[15] W. Masood, H. Rizvi, H. Hasnain, N. Batool, Dust drift shock waves with non-maxwellian ion population in nonuniform collisional dusty plasmas in planetary environments, Astrophys. Space Sci. 345 (2013) 49–55.
[16] J.N. Han, W.S. Duan, J.X. Li, Y.L. He, J.H. Luo, Y.G. Nan, et al., Study of nonlinear electron-acoustic solitary and shock waves in a dissipative, nonplanar space plasma with superthermal hot electrons, Phys. Plasmas 21 (1) (2014) 012102.
[17] P. Shukla, A. Mamun, BOOK REVIEW: introduction to dusty plasma physics, Plasma Phys. Control. Fusion 44 (3) (2002) 395.
[18] N. Rubab, G. Murtaza, Dust-charge fluctuations with non-Maxwellian distribution functions, Phys. Scr. 73 (2) (2006) 178.
[19] M. Hellberg, R. Mace, Generalized plasma dispersion function for a plasma with a kappa-Maxwellian velocity distribution, Phys. Plasmas 9 (5) (2002) 1495–1504.
[20] V.M. Vasyliunas, A survey of low-energy electrons in the evening sector of the magnetosphere with OGO 1 and OGO 3, J. Geophys. Res. 73 (9) (1968) 2839–2884.
[21] U. Zakir, Q. Haque, A. Qamar, A.M. Mirza, Ion-temperature-gradient driven modes in dust-contaminated plasma with nonthermal electron distribution and dust charge fluctuations, Astrophys. Space Sci. 350 (2014) 565–572.
[22] A. Shah, R. Saeed, Nonlinear Korteweg–de Vries–Burger equation for ion-acoustic shock waves in the presence of kappa distributed electrons and positrons, Plasma Phys. Control. Fusion 53 (9) (2011) 095006.
[23] S.K. Mishra, S. Misra, M.S. Sodha, Charging kinetics of dust particles in a non-Maxwellian Lorentzian plasma, Eur. Phys. J. D 67 (2013) 1–10.
[24] M.R. Jana, A. Sen, P.K. Kaw, Collective effects due to charge-fluctuation dynamics in a dusty plasma, Phys. Rev. E 48 (1993) 3930–3933, https://link.aps.org/doi/10.1103/PhysRevE.48.3930.
[25] W.F. El-Taibany, Nonlinear dust acoustic waves in inhomogeneous four-component dusty plasma with opposite charge polarity dust grains, Phys. Plasmas 20 (9) (2013) 093701, http://dx.doi.org/10.1063/1.4820939.
[26] H. Washimi, T. Taniuti, Propagation of ion-acoustic solitary waves of small amplitude, Phys. Rev. Lett. 17 (1966) 996–998, https://link.aps.org/doi/10.1103/PhysRevLett.17.996.
[27] K. Oldham, J. Spanier, The Fractional Calculus Theory and Applications of Differentiation and Integration to Arbitrary Order, Elsevier, 1974.
[28] N. Sene, Double integration for the fractional advection-dispersion equation with nonsingular derivative, in: Applications of Fractional Calculus to Modeling in Dynamics and Chaos, Chapman and Hall/CRC, 2022, pp. 331–352.
[29] K. Aziz, K. Abbas, M. Sinan, Ion temperature gradient modes driven soliton and shock by reduction perturbation method for electron-ion magneto-plasma, Math. Model. Numer. Simul. Appl. 2 (1) (2022) 1–12.
[30] P. Samanta, A. De, S. Dey, D. Maity, A. Ghosh, S. Chandra, Nonlinear excitations in dust-ion acoustic waves and the formation of rogue waves in stable parametric region in a 3-component degenerate plasma, Afr. Rev. Phys. 15 (2021) 10–17.
[31] H. Khan, J.F. Gomez-Aguilar, A. Khan, T.S. Khan, Stability analysis for fractional order advection–reaction diffusion system, Physica A: Statistical Mechanics and Its Applications 521(C) (3–4) (2019) 737–751.
[32] J.H. He, Homotopy perturbation technique, Comput. Methods Appl. Mech. Engrg. 178 (3–4) (1999) 257–262.
[33] S. Sarkar, A. Sett, S. Pramanick, T. Ghosh, C. Das, S. Chandra, Homotopy study of spherical ion-acoustic waves in relativistic degenerate galactic plasma, IEEE Trans. Plasma Sci. 50 (6) (2022) 1477–1487.
[34] C. Das, S. Chandra, B. Ghosh, Amplitude modulation and soliton formation of an intense laser beam interacting with dense quantum plasma: Symbolic simulation analysis, Contrib. Plasma Phys. 60 (8) (2020) e202000028.

[35] S. Rezaei, S. Rezapour, J. Alzabut, R. de Sousa, B. Alotaibi, S. El-Tantawy, Some novel approaches to analyze a nonlinear Schrödinger's equation with group velocity dispersion: Plasma bright solitons, Results Phys. 35 (2022) 105316.

[36] M. Adamu, K.U. Rehman, Y.E. Ibrahim, W. Shatanawi, Predicting abrasion resistance of concrete containing plastic waste, fly ash, and graphene nanoplatelets using an artificial neural network and response surface methodology, AIP Adv. 13 (9) (2023) 095108.

[37] M. Sinan, A. Khan, Analytic approximate solution of rabies transmission dynamics using homotopy perturbation method, Matrix Sci. Math. (MSMK) 4 (1) (2020) 01–05.

[38] A. Ali, M.Y. Khan, M. Sinan, F. Allehiany, E.E. Mahmoud, A.H. Abdel-Aty, et al., Theoretical and numerical analysis of novel COVID-19 via fractional order mathematical model, Results Phys. 20 (2021) 103676.